ISSN 0021-3640, JETP Letters, 2020, Vol. 111, No. 3, pp. 151–156. © Pleiades Publishing, Inc., 2020.
Russian Text © The Author(s), 2020, published in Pis'ma v Zhurnal Eksperimental'noi i Teoreticheskoi Fiziki, 2020, Vol. 111, No. 3, pp. 166–172.

CONDENSED MATTER

Effect of Barium Codoping on Superconductivity in $Sr_xBi_2Se_3$

A. Yu. Kuntsevich[a, b, *], G. V. Rybal'chenko[a], V. P. Martovitskii[a], M. I. Bannikov[a], Yu. G. Selivanov[a], S. Yu. Gavrilkin[a], A. Yu. Tsvetkov[a], and E. G. Chizhevskii[a]

[a] *Lebedev Physical Institute, Russian Academy of Sciences, Moscow, 119991 Russia*
[b] *Moscow Institute of Physics and Technology (National Research University), Dolgoprudnyi, Moscow region, 141700 Russia*
**e-mail: alexkun@lebedev.ru*

Received December 9, 2019; revised December 18, 2019; accepted December 18, 2019

A structural reason for superconductivity in a Cu-, Sr-, or Nb-atom-doped Bi_2Se_3 topological insulator is still unclear. To understand this reason, a codoping approach has been developed and $Ba_ySr_xBi_2Se_3$ single crystals with different x and y values have been grown. The composition and structural and transport properties of the grown crystals have been studied. With X-ray diffraction data, it has been shown that barium and strontium intercalate the system, although barium is present in the structure in a very small amount. The addition of barium surprisingly destroys superconductivity, slightly changing the lattice constants, the strontium doping level of the crystal matrix, and the electron density. Thus, a key role of a certain coordination arrangement of positions of strontium atoms between Bi_2Se_3 quintuples for achieving superconductivity in this material has been demonstrated.

DOI: 10.1134/S002136402003008X

According to the Bardeen–Cooper–Schrieffer (BCS) theory of superconductivity [1], the critical temperature of superconducting transition T_c should exponentially depend on the density of states on the Fermi level. Consequently, the observation of superconductivity with $T_c \sim 3$ K in electron-doped narrow-band semiconductors $A_xBi_2Se_3$ (A = Cu, Sr, Nb) [2–4], where only the very bottom of the conduction band is filled, is mysterious.

The authors of [5, 6] assumed that this unusual superconductivity demonstrates pairing with an odd parity (triplet p-wave). Pairing itself is due to phonons with low momenta k [7–9]. These assumptions are justified by a number of phenomenological observations: (i) the nematicity of superconductivity, i.e., the appearance of the direction of the highest critical field H_{c2} obviously breaking trigonal crystal symmetry [4, 10, 11], in particular, the occurrence of oval Abrikosov vortices [12]; (ii) the appearance of an additional Knight shift below T_c, which is also nematic [13] and indicates a nonzero spin of Cooper pairs; and (iii) a singularity in tunnel characteristics at zero shift [12, 14], which is attributed to Majorana fermions. The status of this field of science is most completely reviewed in [15].

This superconductivity is an enigma at the structural level. Many simple questions remain unanswered. For example, why do certain dopants initiate superconductivity in Bi_2Se_3, whereas other dopants do not? Where are these dopants located in the lattice? Most studies indicate that atoms of a metal dopant are located between Bi_2Se_3 quintuple layers [16–18], but it is unknown what particular coordination position they occupy and why this results in superconductivity. To solve these problems, we study a strontium-doped Bi_2Se_3 system. The $Sr_xBi_2Se_3$ compound has the best crystal perfection (confirmed by X-ray diffractometry), nearly 100% of the superconductivity phase volume, the best homogeneity, and the highest stability [19–21]. Although $Cu_xBi_2Se_3$ was discovered first and was actively studied, it is rather inhomogeneous [12], has a small fraction of the superconductivity volume [16], and demonstrates the degradation of superconducting properties with time [3]. Data on niobium-doped Bi_2Se_3 obtained by different groups are rather contradictory [4, 17]; in particular, good single crystals without admixture of additional phases have not yet been reported.

The superconducting properties of known layered high-T_c superconductors such as $YBa_2Cu_3O_{7-x}$ or $Ba_xK_{1-x}Fe_2As_2$ are controlled by the degree of doping x. The degree of doping specifies primarily the position of the Fermi level, i.e., the density of states in this level, which determines T_c according to the BCS theory. The characteristic carrier densities are several tenths per unit cell. The situation with the superconductivity of doped bismuth chalcogenides is different: the carrier densities are several orders of magnitude

Table 1. Comparative table of the elemental composition, transport properties, and structural parameters of grown crystals: the ratio of resistances *RRR* at 300 and 4 K, the lattice constant $c_{(0015)}$ determined from the (0 0 15) reflection, and the lattice constant $a_{(205)}$ determined from the (2 0 5) reflection using the $c_{(0015)}$; NSC means the absence of superconductivity; the critical temperature is determined in the middle of the resistive transition

Sample no.	Nominal composition	Composition of the crystal phase	n_{Hall}(4 K), 10^{19} cm^{-2}	μ_{Hall}(4 K), $cm^2/(V\,s)$	T_c, K	*RRR*	$c_{(0015)}$, Å	$a_{(205)}$, Å
272	Bi_2Se_3	$Bi_{2.07}Se_3$	0.8	2000	NSC	1.7	28.6343	4.1395
306	$Sr_{0.1}Bi_2Se_3$	$Sr_{0.017}Bi_{2.01}Se_3$	2.2	700	2.7	1.85	28.6596	4.141
317	$Sr_{0.16}Bi_2Se_3$	$Sr_{0.015}Bi_{1.98}Se_3$	2.1	550	2.7	1.4	28.655	4.141
312	$Ba_{0.01}Sr_{0.09}Bi_2Se_3$	$Sr_{0.014}Bi_{2.07}Se_3$	3.3	280	NSC	1.6	28.6535	4.1397
319	$Ba_{0.01}Sr_{0.19}Bi_2Se_3$	$Sr_{0.015}Bi_{2.02}Se_3$	1.6	550	2.7	1.45	28.6538	4.1405
307	$Ba_{0.03}Sr_{0.07}Bi_2Se_3$	$Sr_{0.014}Bi_{1.90}Se_3$	3	360	NSC	1.35	28.6512	4.1400
326	$Ba_{0.03}Sr_{0.19}Bi_2Se_3$	$Sr_{0.015}Bi_{2.00}Se_3$	1.4	300	NSC	1.3	28.651	4.1398
309	$Ba_{0.08}Bi_2Se_3$	$Bi_{1.91}Se_3$	2.8	180	NSC	1.2	28.645	4.1395
316	$Ba_{0.15}Bi_2Se_3$	$Bi_{2.07}Se_3$	0.8	500	NSC	1.45	28.6492	4.1396

lower, and any parameter of the chemical composition that controls the carrier density and superconductivity has not yet been revealed.

It was found in [2, 19] that the average chemical composition of superconducting $Sr_xBi_2Se_3$ is $Sr_{0.07}Bi_2Se_3$ and is slightly sensitive to the nominal strontium content x in the range of $0.1 < x < 0.2$. Partial replacement of a chalcogenide (Se by S) weakly affects the transport properties, including superconducting ones [19]. The addition of Cu [20] increases the Hall carrier density, but in the end suppresses superconductivity. Furthermore, the existence of superconductivity strongly depends on the crystal growth conditions [21, 22]. Thus, the problem of adjustment of this system and understanding of its structure is open.

In this work, we use a new strategy of the partial replacement of Sr by another alkaline-earth element Ba. The ion radius of Ba^{2+} in the octahedral environment (1.35 Å) is noticeably larger than those for Sr^{2+} (1.18 Å) and Bi^{3+} (1.03 Å). For this reason, we believe that the addition of Ba will not concern the sites of the lattice and will promote the broadening of the gap between quintuple layers in the Bi_2Se_3 layered structure, thus changing the strontium susbsystem and all other properties in the z direction.

A series of crystals with different nominal compositions $Ba_ySr_xBi_2Se_3$ were grown from elemental components (99.999% purity Bi and Se, 99.95% purity Sr and Ba) by means of the modified Bridgman method. Chemical elements in the required molar ratio were placed in quartz ampoules in a glove box with an inert atmosphere, which were then evacuated and sealed. Synthesis was performed at 850°C for 24 h with periodic shaking of the ampoule. Further, the melt was cooled to 620°C at a rate of ~2 K/h with the subsequent annealing at 620°C for 48 h and quenching in ice water. The crystals had a shiny surface and were easily cleaved along the basal plane (see [23]). The results of the study of the resulting crystals by various methods are summarized in Table 1 and are discussed below.

The surfaces of the (001) cleavage for all crystals were analyzed in a Jeol JSM-7001F scanning electron microscopy with the subsequent mapping of the elemental composition by means of an INCAx-act energy dispersive X-ray (EDX) analyzer (Oxford Instruments). The accelerating voltage for imaging, mapping, and determining the elemental composition was 25 kV and the beam current was 0.1 mA.

The cleavage plane for non-codoped $Sr_xBi_2Se_3$ samples had some morphological imperfections, as shown in Fig. 1a. The elemental maps in Figs. 1b–1d show that strontium is distributed nonuniformly and is concentrated in the places of the nucleation of the second phase. As we showed in [20], just the main volume of the crystal, rather than strontium-enriched regions of the second phase, contributes to X-ray diffraction and superconductivity.

To determine the composition of this crystalline phase, we took a sample of about 20 points in places of the sample (e.g., marked by crosses in Fig. 2b) where segregation of the metallic impurity was not observed. The composition at each point was determined by collecting the spectrum for 40 min; further, averaging over the points was performed. The composition thus determined is given in the column "Composition of the crystal phase" in Table 1. This composition for non-codoped samples approximately corresponds to $\sim Sr_{0.02}Bi_2Se_3$, which significantly differs from the nominal one.

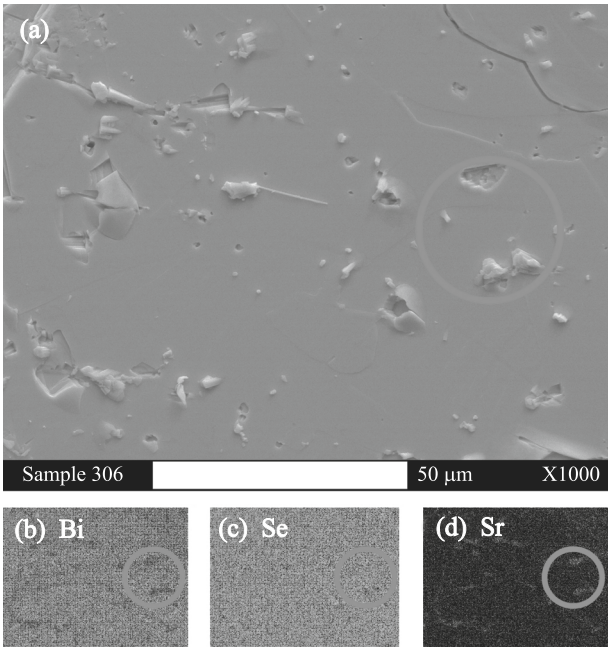

Fig. 1. (Color online) (a) Scanning electron microscopy image of the (0 0 1) cleavage of sample no. 306 with the nominal composition $Sr_{0.1}Bi_2Se_3$ and (b–d) elemental distribution maps. The circles indicate examples of structurally separated regions with Sr excess.

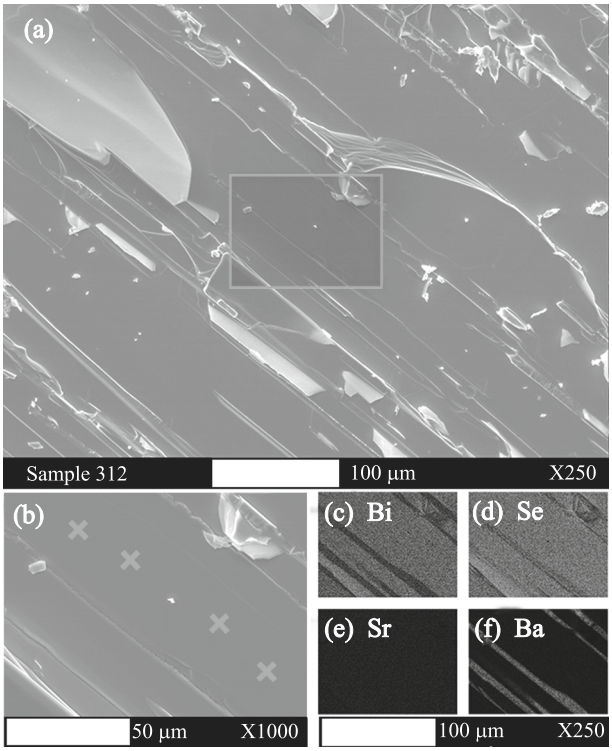

Fig. 2. (Color online) (a) Scanning electron microscopy image of the (0 0 1) cleavage of sample no. 312 with the nominal composition $Ba_{0.01}Sr_{0.1}Bi_2Se_3$. The rectangle indicates the mapping region. (b) Magnified mapping region, where crosses marks examples of points at which the composition was analyzed. (c–f) Elemental maps.

The cleavages of doped (and Ba-codoped) crystals are similar. The energy dispersive analysis did not immediately detect barium along the steps of the cleavages. After searches with reduction of the scanning scale, we succeeded in detecting regions in the crystal where barium is segregated. Figure 2 shows (a, b) scanning electron microscopy images and (c–e) elemental maps of the cleavage of sample no. 312 with the nominal composition $Ba_{0.01}Sr_{0.1}Bi_2Se_3$. The concentration of Ba in segregates is as high as 6 at %, whereas its nominal concentration is 0.2 at %. Thus, the absence of Ba in the main volume of the crystal within the resolution of the elemental analysis is easily explained. Another property is more interesting: the addition of Ba to the system slightly reduces the concentration of Sr and visually suppresses the formation of Sr-enriched microinclusions; indeed, the composition of the crystalline phase in sample no. 312 approximately corresponds to $\sim Sr_{0.014}Bi_2Se_3$. These observations mean that the addition of Ba slightly suppresses the incorporation of Sr into the crystalline phase of Bi_2Se_3 and makes the distribution of Sr atoms in the matrix more uniform.

We also grew $Ba_yBi_2Se_3$ crystals with a large nominal Ba content ($y = 0.07$ and 0.15 for samples no. 309 and no. 316, respectively). Barium in these samples was also not detected in the bulk of crystals, but was found only in inclusions. This indicates that barium even without strontium is very weakly soluble in the solid phase of Bi_2Se_3. This property shows that just the large ion radius of Ba likely prevents its introduction to the intercalating position, whereas Sr can occupy coordination positions between Bi_2Se_3 quintuple layers of a growing crystal.

To reveal the structural features of Ba-doped crystals, we performed X-ray diffraction studies. Although the structure of the crystal is trigonal (space group $R3m$), it is more convenient to describe the layered structure using hexagonal notation for crystallographic planes (abc), where the third index $i \equiv -a - b$ is omitted.

Review 2θ scans of the crystals with different compositions are shown in Figs. 3a–3d. Narrow lines demonstrate a high structural perfection and rhombohedral tetradymite structure. The second phase is formed in samples with a high nominal barium content ($y \sim 0.07$—0.15). The introduction of Sr to binary Bi_2Se_3 reduces the structural perfection of the crystalline phase, as indicated by the relative decrease in the intensity of (0 0n) reflections with large n values. It is interesting that the structural perfection in crystals with the simultaneous Ba and Sr doping increases (see Fig. 3d). This is in agreement with the fact that barium prevents the formation of microinclusions of the

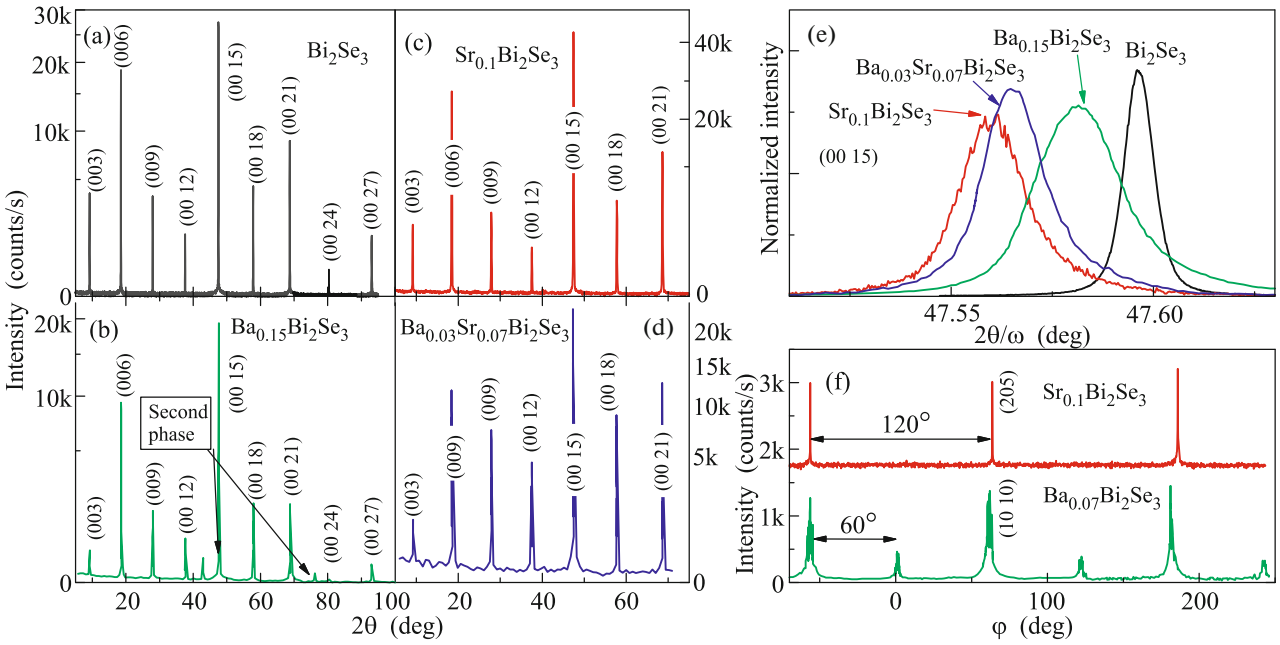

Fig. 3. (Color online) (a–d) Review 2θ/ω diffraction patterns of crystals with indicated compositions grown in this work. Peaks from another phase are additionally shown in panel (b). (e) High-resolution 2θ/ω curves on the (0 0 15) reflection recorded for the same samples with the third analyzer crystal. (f) ϕ-scanning curves on asymmetric reflections with the third-order symmetry for the (upper curve) $Sr_{0.1}Bi_2Se_3$ and (lower curve) $Ba_{0.07}Bi_2Se_3$ samples.

strontium-enriched second phase. Nevertheless, samples doped only with barium in an excess amount (e.g., sample no. 316, see Fig. 3b) are the most disordered.

For the quantitative characterization of the effect of impurities on the structure, we performed adjustment to the most intense blocks, as explained in [23, 24], and recorded 2θ/ω curves on the (2 0 5), (0 0 15), and (1 1 15) reflections with the tripple crystal analyzer. Such curves for the (0 0 15) reflection are shown in Fig. 3e. It is noteworthy that the angular position of the reflection peak is unambiguously related to the lattice parameter c. It is clearly seen that the lattice constant c is maximal and minimal for the $Sr_{0.1}Bi_2Se_3$ and Bi_2Se_3 crystals, respectively. It is known that the saturation of the strontium content and the maximum lattice constant c in $Sr_xBi_2Se_3$ occurs at the nominal value $x > 0.06$ [2]. The addition of barium at the same total content $x + y = 0.1$ noticeably reduces the lattice parameter c. Since the ion radius of Ba is larger, this can be explained only by a decrease in the resulting strontium concentration in the crystal.

However, even in the crystal with barium without strontium, where the elemental analysis does not detect barium, the lattice constant c is much larger than that in Bi_2Se_3. The half-width of the 2θ/ω scanning curve increases from $\Delta(2\theta)_{(0015)} = 0.009°$ for pure Bi_2Se_3 to $\Delta(2\theta)_{(0015)} = 0.025°$ for the barium-doped sample. Since the lattice constant $a_{(205)}$ in the basal plane is almost the same in the undoped and barium-doped samples (see Table 1), it can be concluded that barium in some amount enters, although with difficulty and nonuniformly, intercalated positions between quintuple layers. The formation of 60° twins was observed in the same samples with barium, according to the appearance of three additional peaks on the φ-scanning curve (Fig. 3f). All these features confirm that barium prevents the intercalation of strontium into the lattice and itself enters in a very small amount.

Transport measurements were also performed with all samples: 5 × 1 × 0.3-mm rectandular pieces were cleaved, and the resesitivity and Hall effect in fields up to 2 T were measured. The measurements were performed in the temperature range of 1.8–300 K at an alternating current (~100 μm, frequency of 30–170 Hz) using PPMS-9 and CFMS-16 cryostats. The resistances of the painted contacts were tens of ohms. The temperature dependences of the resistivity are exemplified in Figs. 4a and 4b. It is seen that barium suppresses superconductivity, slightly changing the superconducting transition temperature. A small shift of the beginning of the transition in codoped sample no. 319 is within the spread of T_c characteristic of this material (see Fig. 6b in [20]). A slow decrease in the resistivity of sample no. 319 indicates a significant decrease in the fraction of the superconductivity phase.

All samples demonstrated reasonably close mobilities and residual-resistance ratio (or the ratio of the

resistivity at 300 K to the resistivity at liquid helium temperature) *RRR* ~ 1.5. This is in agreement with the segregation of barium: it sediments in large rare inclusions, so that the number of scattering nano- and microcenters does not increase. It is noteworthy that samples consist of blocks, and their resistivity includes the resistivity of the bulk of the crystal itself and, significantly, interblock boundaries [20, 23]. As a result, the observed *RRR* and mobility μ values can differ by 25–30% even for samples separated from the same crystal. Correspondingly, the quantitative conclusions from the μ and *RRR* values will be unreliable.

The Hall concentration weakly depends on a particular position of blocks in the sample and on the temperature. This means that the Fermi level certainly lies in the conduction band far from impurity levels. Sample no. 316 doped only with barium exhibited even some decrease in the concentration compared to $Sr_xBi_2Se_3$. Shubnikov–de Haas oscillations indicate a comparatively high structural quality and similar electronic parameters (Fig. 4c). Oscillations in codoped and non-codoped samples begin in the same field and have close frequencies. All these data indicate that the location of strontium in certain places of the lattice is responsible for superconductivity and partially for the concentration. Barium reduces the concentration of strontium and, according to X-ray data, partially enters the lattice itself, so that the resulting change in the concentration is insignificant. This means that the key reason for superconductivity is a certain specific structure in the arrangement of impurity atoms rather than the position of the Fermi level.

DISCUSSION OF THE RESULTS

In contrast to all previous works, where the strontium content in $Sr_xBi_2Se_3$ crystals was not controlled and was determined by its solubility in the crystal phase, we were able in this work to slightly reduce the strontium content by means of cooping. According to our data, superconductivity is suppressed. It is noteworthy that the suppression of superconductivity is not accompanied by change in T_c. To explain such extraordinary properties, it is impossible to exclude the possibility of ordering of strontium at a submicron scale. In this case, a seemingly uniform elemental distribution map can really be nonuniform. It is very difficult to establish such a possibility with the current level of analytical methods. Indeed, the amount of strontium in "superconducting" positions in the crystal is very small (less than 0.4 at %) and it is located between quintuple Bi_2Se_3 layers, i.e., has weak bonds with the lattice. At the same time, the appearance of superconductivity is likely finely related to the Sr concentration in the matrix. Indeed, superconductivity in codoped samples with the same nominal barium content $y = 0.01$ appears when the nominal strontium

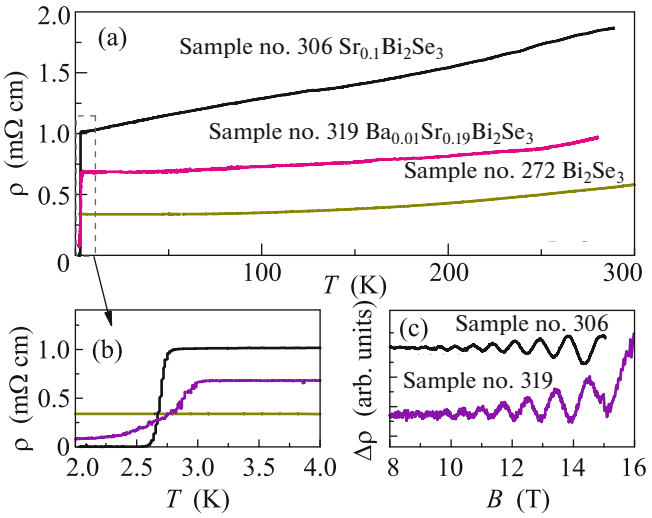

Fig. 4. (Color online) (a) Temperature dependences of the resistivity of several crystals with indicated compositions. (b) Magnified low-temperature part. (c) Magnetic-field dependences of the resistivity at a temperature of 2 K with Shubnikov–de Haas oscillations for samples no. 306 and no. 319.

content increases from $x = 0.09$ to $x = 0.19$ (see samples no. 312 and no. 319 in Table 1).

Calcium is the only remaining alkaline-earth element that can be used to dope the Bi_2Se_3 system (Be, Mg, and Ra are not considered because they have fundamentally different properties). Calcium has the smallest radius; for this reason, as shown in [25, 26], it not only enters between Bi_2Se_3 quintuple layers but also substitutes bismuth in quintuple layers themselves, leading to the *p*-type conductivity. Calcium also tends to segregation [25]. We thereby believe that calcium, as a codopant, will not promote the appearance of superconductivity in the $Sr_xBi_2Se_3$ system. Our work has revealed the general tendency in a series of alkaline-earth dopants of Bi_2Se_3: calcium, being the smallest of them, not only enters between layers but also substitutes bismuth; strontium, as a larger element, does not enter quintuple layers themselves but intercalates; and barium, being the largest of them, hardly intercalates (poorly soluble in the solid phase of the tetradymite structure). It is noteworthy that the replacement of bismuth is characteristic of metallic impurities in this system [27]. The statement that it is not the main doping mechanism for alkaline-earth metals requires further study. A tendency to segregation is also manifested for various metallic impurities in Bi_2Se_3 [28].

CONCLUSIONS

To summarize, we have presented a comparative structural proof through barium codoping that strontium in Bi_2Se_3 is located between quintuple layers. We

have shown that barium slightly reduces the strontium content in the crystal phase, enters the lattice in a very small amount, but strongly suppresses superconductivity. The Hall concentration and lattice constant c are insensitive to barium addition. This indicates that the key factor for $Sr_xBi_2Se_3$ is a certain structural configuration of metal atoms in the van der Waals gap between quintuple layers rather than the concentration of dopants or free carriers as for other superconducting systems.

ACKNOWLEDGMENTS

The measurements were performed at the Shared Facility Center, Lebedev Physical Institute, Russian Academy of Sciences.

FUNDING

This work was supported by the Russian Science Foundation, project no. 17-12-01544.

REFERENCES

1. J. Bardeen, L. N. Cooper, and J. R. Schrieffer, Phys. Rev. **108**, 1175 (1957).
2. Z. Liu, X. Yao, J. Shao, M. Zuo, L. Pi, S. Tan, C. Zhang, and Y. Zhang, J. Am. Chem. Soc. **137**, 10512 (2015).
3. Y. S. Hor, A. J. Williams, J. G. Checkelsky, P. Roushan, J. Seo, Q. Xu, H. W. Zandbergen, A. Yazdani, N. P. Ong, and R. J. Cava, Phys. Rev. Lett. **104**, 057001 (2010).
4. T. Asaba, B. J. Lawson, C. Tinsman, L. Chen, P. Corbae, G. Li, Y. Qiu, Y. S. Hor, L. Fu, and L. Li, Phys. Rev. X **7**, 011009 (2017).
5. L. Fu and E. Berg, Phys. Rev. Lett. **105**, 097001 (2010).
6. L. Fu, Phys. Rev. B **90**, 100509(R) (2014).
7. X. Wan and S. Y. Savrasov, Nat. Commun. **5**, 4144 (2014).
8. P. M. R. Brydon, S. Das Sarma, H.-Y. Hui, and J. D. Sau, Phys. Rev. B **90**, 184512 (2014).
9. J. Wang, K. Ran, S. Li, Z. Ma, S. Bao, Z. Cai, Y. Zhang, K. Nakajima, S. Ohira-Kawamura, P. Čermàk, A. Schneidewind, S. Y. Savrasov, X. Wan, and J. Wen, Nat. Commun. **10**, 2802 (2019).
10. Y. Pan, A. M. Nikitin, G. K. Araizi, Y. K. Huang, Y. Matsushita, T. Naka, and A. de Visser, Sci. Rep. **6**, 28632 (2016).
11. S. Yonezawa, K. Tajiri, S. Nakata, Y. Nagai, Z. Wang, K. Segawa, Y. Ando, and Y. Maeno, Nat. Phys. **13**, 123 (2017).
12. R. Tao, Y.-J. Yan, X. Liu, Z.-W. Wang, Y. Ando, Q.-H. Wang, T. Zhang, and D.-L. Feng, Phys. Rev. X **8**, 041024 (2018).
13. K. Matano, M. Kriener, K. Segawa, Y. Ando, and G. Zheng, Nat. Phys. **12**, 852 (2016).
14. S. Sasaki, M. Kriener, K. Segawa, K. Yada, Y. Tanaka, M. Sato, and Y. Ando, Phys. Rev. Lett. **107**, 217001 (2010).
15. S. Yonezawa, Condens. Matter **4**, 2 (2019).
16. M. Kriener, K. Segawa, Z. Ren, S. Sasaki, S. Wada, S. Kuwabata, and Y. Ando, Phys. Rev. B **84**, 054513 (2011).
17. K. Kobayashi, T. Ueno, H. Fujiwara, T. Yokoya, and J. Akimitsu, Phys. Rev. B **95**, 180503(R) (2017).
18. S.-H. Yu, T. L. Hung, M.-N. Ou, M. M. C. Chou, and Y.-Y. Chen, Phys. Rev. B **100**, 174502 (2019).
19. H. Huang, J. Gu, M. Tan, Q. Wang, P. Ji, and X. Hu, Sci. Rep. **7**, 45565 (2017).
20. A. Yu. Kuntsevich, V. P. Martovitskii, G. V. Rybalchenko, Yu. G. Selivanov, M. I. Bannikov, O. A. Sobolevskiy, and E. G. Chigevskii, Materials **12**, 3899 (2019).
21. S. O. Volosheniuk, Yu. G. Selivanov, M. A. Bryzgalov, V. P. Martovitskii, and A. Yu. Kuntsevich, J. Appl. Phys. **125**, 095103 (2019).
22. Z. Li, M. Wang, D. Zhang, N. Feng, W. Jiang, C. Han, W. Chen, M. Ye, C. Gao, J. Jia, J. Li, S. Qiao, D. Qian, B. Xu, H. Tian, and B. Gao, Phys. Rev. Mater. **2**, 014201 (2018).
23. A. Yu. Kuntsevich, M. A. Bryzgalov, V. A. Prudkoglyad, V. P. Martovitskii, Yu. G. Selivanov, and E. G. Chizhevskii, New J. Phys. **20**, 103022 (2018).
24. A. Yu. Kuntsevich, M. A. Bryzgalov, V. P. Martovitskii, R. S. Akzyanov, Yu. G. Selivanov, and A. L. Rakhmanov, Phys. Rev. B **100**, 224509 (2019).
25. Y. S. Hor, A. Richardella, P. Roushan, Y. Xia, J. G. Checkelsky, A. Yazdani, M. Z. Hasan, N. P. Ong, and R. J. Cava, Phys. Rev. B **79**, 195208 (2009).
26. J. Moon, N. Koirala, M. Salehi, W. Zhang, W. Wu, and S. Oh, Nano Lett. **18**, 820 (2018).
27. E. T. Kulatov, V. N. Men'shov, V. V. Tugushev, and Yu. A. Uspenskii, JETP Lett. **109**, 102 (2019).
28. L. N. Oveshnikov, V. A. Prudkoglyad, Yu. G. Selivanov, E. G. Chizhevskii, and B. A. Aronzon, JETP Lett. **106**, 526 (2017).

Translated by R. Tyapaev